# Bias-Stress-Stable Solution-Processed Oxide Thin Film Transistors

**Youngmin Jeong,[†] Changdeuck Bae,[†] Dongjo Kim,[†] Keunkyu Song,[†] Kyoohee Woo,[†] Hyunjung Shin,[‡] Guozhong Cao,[§] and Jooho Moon*[,†]**

Department of Materials Science and Engineering, Yonsei University, 134 Shinchon-dong Seodaemun-gu, Seoul 120-749, Korea, School of Advanced Materials Engineering, Kookmin University, Jeongneung-gil 77, Seoul 136-702, Korea, and Department of Materials Science and Engineering, University of Washington, Seattle, Washington 98195

**ABSTRACT** We generated a novel amorphous oxide semiconductor thin film transistor (AOS-TFT) that has exellent bias-stress stability using solution-processed gallium tin zinc oxide (GSZO) layers as the channel. The cause of the resulting stable operation against the gate bias-stress was studied by comparing the TFT characteristics of the GSZO layer with a tin-doped ZnO (ZTO) layer that lacks gallium. By photoluminescence, X-ray photoelectron, and electron paramagnetic resonance spectroscopy, we found that the GSZO layer had a significantly lower oxygen vacancy, which act as trap sites, than did the ZTO film. The successful fabrication of a solution-processable GSZO layer reported here is the first step in realizing all-solution-processed transparent flexible transistors with air-stable, reproducible device characteristics.

**KEYWORDS:** amorphous oxide semiconductor • bias-stress stability • solution-processed transistor • gallium tin zinc oxide

Amorphous oxide semiconductors (AOSs) are a promising active layer for transparent, flexible thin film transistors (TFTs) (1−3). Solution processing for the formation of AOS layers is likely a viable alternative to vacuum deposition techniques with respect to processing temperature and cost, as well as having direct-write capabilities, such as in inkjet printing (4, 5). However, solution-processed AOS TFTs suffer from severe bias-stress instability for device operation because of inherently rich and undefined defect states, thus inhibiting reproducible, reliable performance. Here, we report on the generation of solution-processed gallium tin zinc oxide (GSZO) TFTs that exhibit superior stability against electrical stress during device operation under ambient conditions. By electron paramagnetic resonance, photoluminescence, and X-ray photoelectron assays, we compared GSZO with gallium-free tin-doped ZnO (ZTO) layers, and we suggest that oxygen vacancies and the control of them are key to producing reproducible AOS channel layers by solution processing.

Thanks to huge efforts in the development of CMOS-compatible processes for AOS deposition, high mobility and on−off current ratios were typically achieved in the ranges of 5−20 $cm^2\ V^{-1}\ s^{-1}$ and $1 \times 10^6$ to $1 \times 10^7$, respectively, using ZnO-based TFTs (6−10). Alternatively, AOS layers from solution processes require minimal material consumption and allow for large area coating, direct writing and high throughput capabilities. We and others have reported AOS TFT performances that are comparable with those from vacuum deposition techniques, using solution-processed ZTO transistors with a mobility of 1.14 $cm^2\ V^{-1}\ s^{-1}$ and an on−off current ratio of $\sim 1 \times 10^6$ (11). In our previous work, we observed bias-stress instability of solution-processed ZTO transistors with the gate voltage applied (12). The application of positive bias-stress displaces the transfer characteristics in the positive direction without changing the field effect mobility or the subthreshold swing parameter. By investigating the time dependence and the value of the gate stress, we concluded that the instability of the ZTO device was responsible for temporal charge trapping at the interface and/or in the ZTO channel region. We suspect that oxygen vacancies act as major trap sites. Therefore, to improve the bias-stress stability of solution-processed AOS TFTs, we must reduce defect states, such as oxygen vacancies, in the solution-processed layers.

In the present work, we generated solution-processed AOS TFTs using GSZO layers as the channel. Importantly, these AOS TFTs had excellent bias-stress stability during device operation under ambient conditions. The cause of the bias-stress stability was investigated by comparing GSZO and ZTO layers. The creation and quantity of oxygen vacancies generated from the addition of Ga ions were probed with concrete spectroscopic results. By photoluminescence (PL) and X-ray photoelectron spectroscopy (XPS), we observed a general trend toward suppression of oxygen-related defects upon the addition of Ga (13). Electron paramagnetic resonance (EPR) of both the GSZO and ZTO layers allowed us to quantify the oxygen vacancies. Because of the reproducible TFT characteristics, the strategy presented here

* To whom correspondence should be addressed. E-mail: jmoon@yonsei.ac.kr.
Received for review November 12, 2009 and accepted February 22, 2010
[†] Yonsei University.
[‡] Kookmin University.
[§] University of Washington.
DOI: 10.1021/am900787k

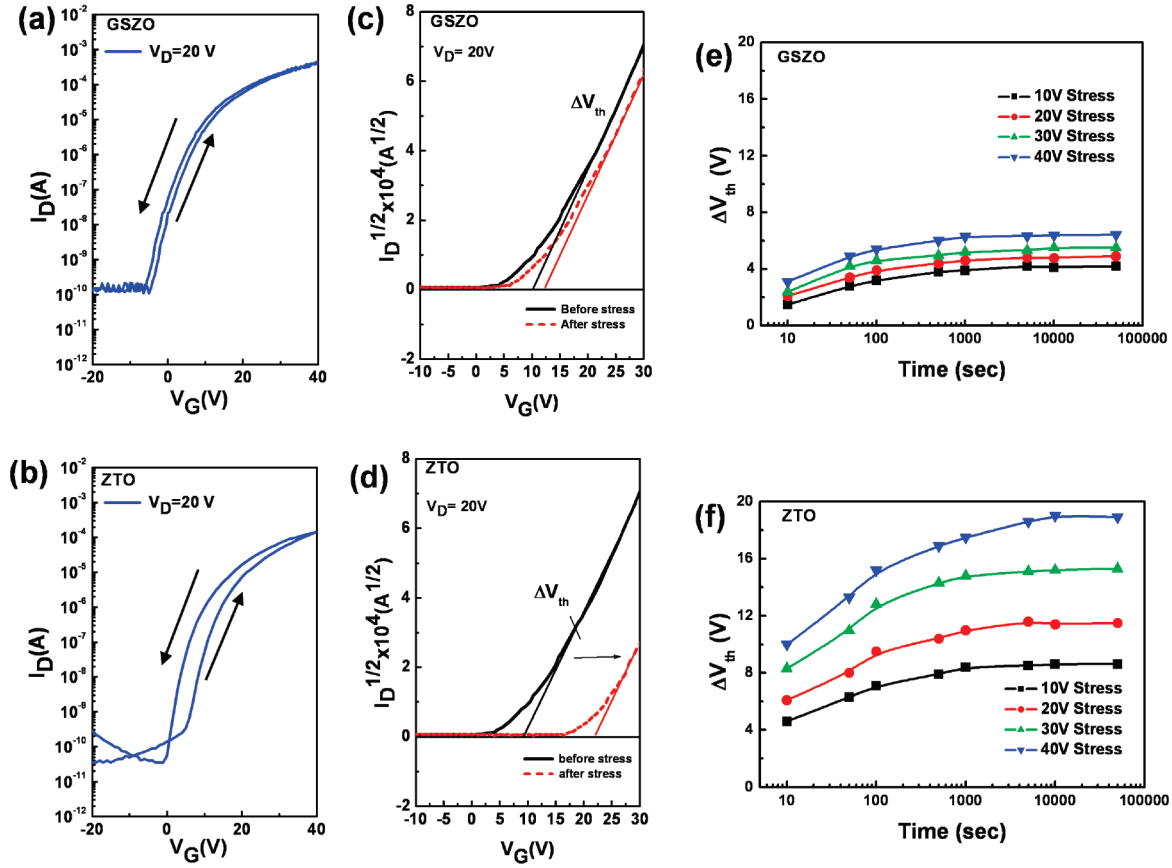


**FIGURE 1. Typical transfer characteristics of as-prepared (a) GSZO and (b) ZTO transistors. The $\sqrt{I_D}$ vs $V_G$ plot to extract the threshold voltage shift for the spin-coated (c) GSZO- and (d) ZTO-TFTs after applying electrical stress with a gate bias of 20 V for 60 min. The dependence of the threshold voltage shift on the duration of the applied gate bias is plotted for different stress voltages. The saturation values of these devices were increased with stress voltages of 10 to 40 V. (e) For GSZO, the graph shows a very similar tendency with (f) ZTO, but the degree of threshold voltage shift at the same duration of shifted voltage values was substantially lower than that for ZTO, verifying that GSZO was a more stable oxide semiconductor compared with ZTO, which resulted from the addition of Ga ions.**

will enable the development of solution-processable high-performance electronic devices for transparent, flexible substrates.

Panels a and b in Figure 1, respectively, show the transfer characteristics of GSZO and ZTO TFTs (see Experimental Section for detailed preparation methods). These devices showed very similar TFT characteristics and exhibited saturation mobilities of 1.0 to 1.2 $cm^2\ V^{-1}\ s^{-1}$, on/off current ratios of $\sim 1 \times 10^6$, and a subthreshold slope of 1.5 V $dec^{-1}$. The threshold gate voltage was positive ($V_{th} = 3$ V), showing that both TFTs operated in the enhancement mode (normally off characteristics). This indicates that doping with Ga ions had no significant effect on the resulting electrical performance of the TFTs. Interestingly, doped Ga ions increased the bias-stress stability of the TFTs, resulting in a large difference between GSZO (threshold voltage shift, $\Delta V_{th}$, of ~2 V) and ZTO ($\Delta V_{th}$ of ~8 V) from their initial transfer characteristics curves (Figure 1a,b). Such an effect was further visualized by plotting the square root of the drain current after applying the gate bias (ca. 20 V for 60 min) (Figure 1c,d). Although the application of positive bias-stress resulted in a large displacement ($\Delta V_{th}$ of ~13 V) of the transfer curves in the positive direction for ZTO transistors (Figure 1d), the GSZO transistor had a relatively small $\Delta V_{th}$ of ~4 V, even after applying the same gate voltage stress (Figure 1c). These results indicate that the GSZO transistor has better bias-stress stability with minimal hysteresis and a threshold voltage shift. Panels e and f in Figure 1 summarize the comparison of the device stabilities between ZTO and GSZO TFTs as functions of both bias-stress and its duration.

The fluctuation of the difference in threshold voltage resulting from the bias-stress applied at an appropriate duration could be ascribed to temporal charge trapping at the interface and/or in the AOS channel region (12). Presently, we suspect that oxygen vacancies may act as trap states. To investigate the oxygen vacancies in both the ZTO and GSZO films, we compared the relative ratio of oxygen-related defects by XPS analysis. The XPS peaks for the O1s core level demonstrated three different peaks for both AOS layers (Figure 2a,b), which could be consistently fitted by three near-Gaussians curves, centered at 529.8, 531.3, and 532.4 eV. The dominant peak centered at 529.8 eV (O1) was assigned to the $O^{2-}$ ion in a wurtzite structure surrounded by Zn atoms with their full complement of four nearest neighbor $O^{2-}$ ions (14). The peak at 531.3 eV (O2) was associated with the $O^{2-}$ ion in oxygen-deficient regions. The binding energy peak at 532.4 eV (O3) was attributed to the presence of hydroxyl groups on the surfaces. The peak area at 531.3 eV reflected oxygen vacancies as well as composi-

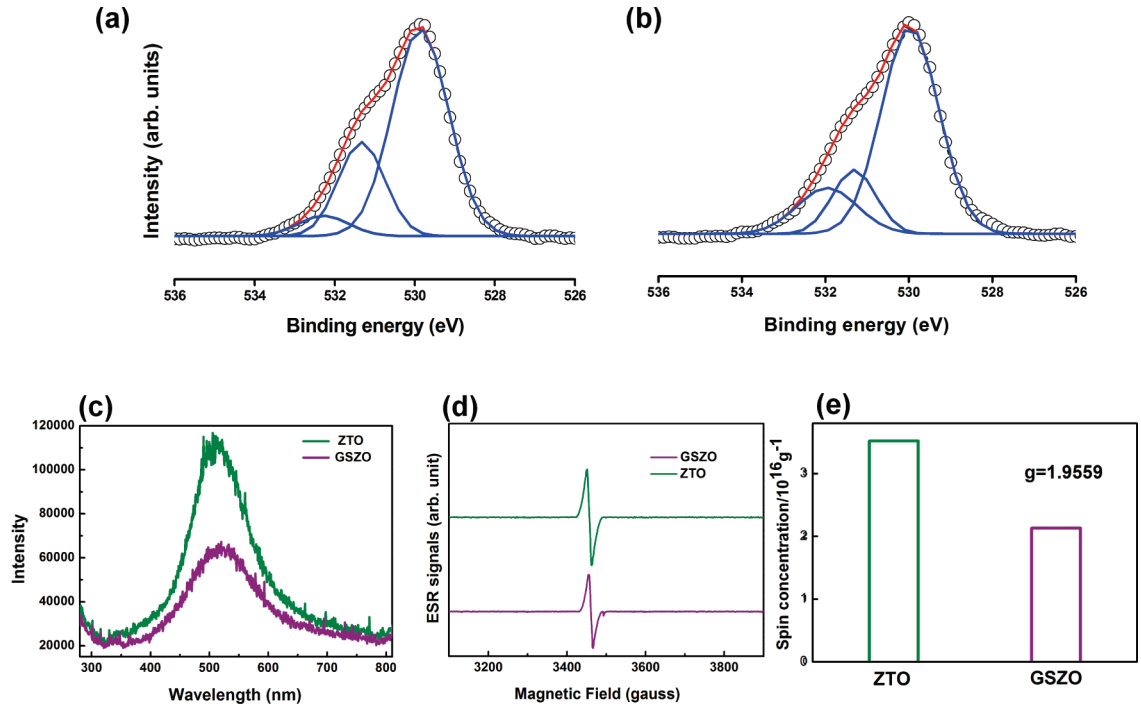


**FIGURE 2. XPS spectra of the O 1s core level line for the solution-processed (a) ZTO and (b) GSZO films. (c) Room-temperature (298 K) photoluminescence spectra of our GSZO and ZTO thin films on quartz glass. (d) X-band EPR spectra of GSZO and ZTO, and (e) spin concentration of the defect centers ($V_{\dot{O}}$) for the line at $g = 1.9559$.**

tion imperfections at the surface. The ratio of the areas (O2/O1) was used to estimate the relative quantity of oxygen deficiencies (15). The O2/O1 ratio was 0.39 for ZTO and 0.21 for GSZO, indicating that ZTO had more oxygen vacancies and contained more trap sites than does GSZO. These results were confirmed by PL analysis (Figure 2c). Luminescence from ZnO-based materials results from the radiative recombination of excitons in surfaces (16). Therefore, the relative intensity of the green emission at about 540 nm using PL spectroscopy correlates with the increases in the concentration of oxygen vacancies as a result of the recombination of electrons trapped at singly ionized oxygen vacancies (Figure 3) (17−19). In other words, gallium suppressed the generation of oxygen vacancies, and the control of oxygen vacancies in sol−gel-processed ZnO-based TFT films was essential to bias-stress stability.

We also assayed the quantities of oxygen vacancies for both AOS films by EPR (Figure 2d). The main $g$-factor values were 1.9559. The resonance position is close to the shallow donor level and is usually assigned to the presence of a singly ionized oxygen vacancy defect ($V_{\dot{O}}$). The spin concentration of the defect centers decreased by a factor of ~0.4 with the resonance intensity at $g = 1.9559$ as the Ga ions were doped (Figure 2e). These quantitative analyses of oxygen vacancies in sol−gel-processed ZTO and GSZO thin films affirmatively demonstrated that the stability of bias-stress was influenced by the amount of oxygen vacancies, and that Ga doping resulted in bias-stress stability by strongly suppressing oxygen vacancy generation. It is noted that the concentration of EPR active oxygen vacancies (~$1 \times 10^{17}$ cm$^{-3}$ in Figure 2e) was quite lower than that of oxygen-related defects from our XPS results when considering the lattice oxygen concentration (~$1 \times 10^{22}$ cm$^{-3}$ in Figure 2b). We

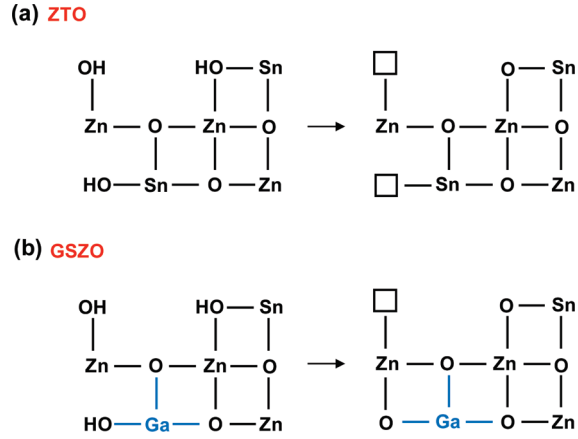


**FIGURE 3. Creation mechanism of oxygen vacancies upon thermal treatment in (a) ZTO and (b) GSZO films (□, oxygen vacancy). Although panel a shows the typical dehydroxylation processes during annealing, the blue lines in b indicate the strong bonding of the doped Ga ion and the oxygen vacancy.**

attributed this discrepancy to the different origins between the EPR active vacancies and the vacancies detected in XPS. The EPR active oxygen vacancies only represent some of the total, i.e., diverse, complex oxygen vacancies in our GSZO.

We proposed a possible mechanism for the formation of different vacancies in the GSZO and ZTO layers to explain the effect of Ga doping in our solution-processed AOS TFTs. It is generally accepted that oxygen vacancies in such systems are produced via poly condensation and dehydroxylation/dehydration processes during the annealing of sol−gel films, as illustrated in Figure 3a (20−23). The surface hydroxyl groups (MOH), including the top and inner pore surfaces, are dehydroxylated and dehydrated upon heat treatment, releasing $H_2O$ (from one hydroxyl + one hydro-

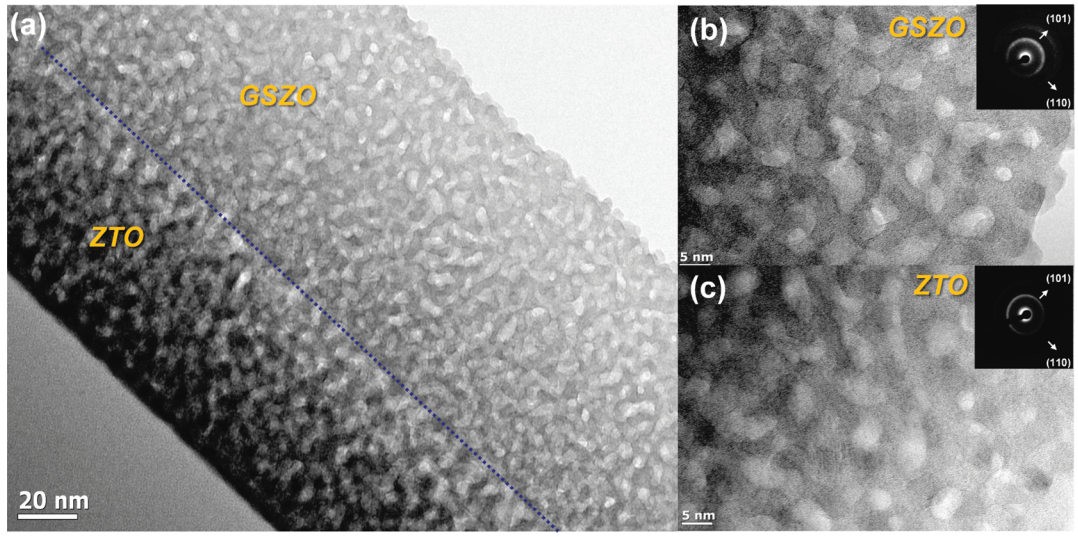


**FIGURE 4. (a) Cross-sectional-view TEM image of the sol−gel-derived GSZO/ZTO films showing microstructures with nanoscale pores inside. The double-layer sample was prepared for TEM observation by a successive spin-coating and annealing. Both the GSZO and ZTO films are composed of an amorphous phase in which 1−2 nm sized crystalline particles of $Zn_2SnO_4$ are embedded. (b, c) Enlarged TEM micrographs of each part, i.e., GSZO and ZTO, respectively. The insets are the corresponding electron diffraction patterns, indicative of the mixed amorphous and crystalline phases with the diffused ring patterns.**

gen) and creating oxygen vacancies on the surfaces (Figure 3a). Because of the bonding strength between gallium and oxygen ions, the addition of Ga precursors into the sols is expected to increase the dehydration probability, rather than reduce the probability of releasing hydroxyl groups, leading to a reduced concentration of oxygen vacancies (compare Figure 3a with 3b). Considering the electronegativity of constituent cations, the relative bonding strengths of oxygen and the cations were estimated using the partial charge model (PCM) (24). The calculated partial charge ($\delta$) of gallium (−0.12) was lower than those of zinc (−0.03) and tin (−0.07). The stronger bonding strength between Ga and the oxygen ions suppressed the creation of oxygen vacancies in the Ga-doped layer, which is in a good agreement with the experimental results.

Finally, Figure 4 shows transmission electron microscopy (TEM) images of ZTO and GSZO films. The results demonstrate the similar porosities between the ZTO and GSZO layers, as determined by the heterogeneity in the TEM contrast. However, the shift in threshold voltage might be influenced by the quality of the thin film itself. For example, nanopores should exist within the solution-processed AOS layer, as gas escape paths from organometallic precursors during annealing. Depending on the preparation methods, in fact, we have observed different characteristics of the threshold voltage shift resulting from the differing pore densities of spin-coated and inkjet-printed devices (15). Therefore, the observed similarity in the pore densities and average dimensions between both layers demonstrates that the difference in threshold voltage shift resulting from the addition of Ga precursors to ZTO is not due to possible artifacts, such as the porous structures of AOS layers.

In summary, we generated solution-processed GSZO TFTs with excellent bias-stress stability and with saturation mobility of up to 1.2 $cm^2\ V^{-1}\ s^{-1}$, on/off current ratios of $\sim 1 \times 10^6$, and a subthreshold slope of 1.5 V $dec^{-1}$. By comparing the GSZO layer with the Ga-free ZTO film, we observed that the former had a significantly lower oxygen vacancy concentration than did the latter. We assayed the plausible cause of the stable operation for both films by photoluminescence, X-ray photoelectron, and electron paramagnetic resonance spectroscopy. The decrease in oxygen vacancies by Ga doping was also explained in terms of the partial charge model. The soultion-processable GSZO layer demonstrated here will enable the development of transparent flexible transistors with air-stable, reproducible device characteristics toward all-solution-processed microelectronics.

## EXPERIMENTAL METHOD

**Preparation of AOS Films and AOS TFTs.** A precursor solution for a ZTO semiconductor was synthesized by a sol−gel process as described previously (11). The generation of GSZO semiconducting solution was identical to that of ZTO except for the addition of the Ga precursor. Zinc acetate dehydrate ($Zn(CH_3COO)_2 \cdot 2H_2O$), tin acetate ($Sn(CH_3COO)_2$), and gallium nitrate hydrate ($Ga(NO_3)_3 \cdot H_2O$) were dissolved in 2-methoxyethanol. The concentration of metal precursors was 0.75 M, and the molar ratio of Ga:Sn:Zn was 0.5:2.8:6.7. Using the precursor solution, we fabricated stagger-type transistors by spin-coating using Al source/drain electrodes. The substrates were cleaned with isopropyl alcohol prior to deposition. The precursor solution was spin-coated at 3000 rpm for 20 s. The resulting films were dried at 100 °C for 90 s to evaporate the solvent and annealed at 500 °C for 4 h in air for complete thermal decomposition of organic residues and metal salts. After annealing, the spin-cast films had thicknesses of ∼ 30 nm, as determined by a surface profiler (Dektak 150, Veeco Instruments Inc.). To fabricate stagger-type TFTs, we vacuum-deposited Al source/drain electrodes to a 50 nm thickness via a shadow mask on top of the GSZO and ZTO layers on the substrates. A postannealing step was then performed at 200 °C for 1 min in a $H_2/N_2$ (5/95 in volume %) atmosphere to improve the electrical performance of the transistor prior to measurement. The film microstructures were investigated by high-resolution transmission electron microscopy (HRTEM, JEM-

4010, JEOL). X-ray photoelectron spectroscopy (XPS, ThermoVG, U.K.), electron paramagnetic resonance (EPR, ESP 300E, Bruker), and photoluminescence spectroscopy (PL, He−Cd laser Darsa, PSI) were used to identify the relative oxygen vacancies in the AOS thin films.

**Electrical Measurements.** All bias-stress measurements were carried out at room temperature in air and in the dark using an Agilent 4155C semiconductor parameter analyzer. Gate biases between 10 and 40 V were applied to the gate contact for various periods up to $5 \times 10^4$ s using a fresh, unstressed device for each stressing condition. Bias-stressing was interrupted at predetermined times in order to measure the transfer characteristics. Saturation mobility ($\mu_{sat}$) and threshold voltage ($V_{th}$) determination were performed in the saturation regime by extracting the slope above $V_{th}$ from the $\sqrt{I_D}$ vs $V_G$ plot and the axis intercept, respectively.

**Acknowledgment.** This research was supported by the Basic Science Research Program through the National Research Foundation of Korea (NRF) funded by the Ministry of Education, Science and Technology (R0A-2005-000-10011-0 and 2009-0086302). It was also partially supported by the Second Stage of the Brain Korea 21 Project.

## REFERENCES AND NOTES

(1) Nomura, K.; Ohta, H.; Takagi, A.; Kamiya, T.; Hirano, M.; Hosono, H. *Nature* **2004**, *432*, 488.
(2) Kumomi, H.; Nomura, K.; Kamiya, T.; Hosono, H. *Thin Solid Films* **2008**, *516*, 1516.
(3) Fortunato, E.; Barquinha, P.; Pimentel, A.; Gonçalves, A.; Marques, A.; Pereira, L.; Martins, R. *Thin Solid Films* **2005**, *487*, 205.
(4) Gates, B. D. *Science* **2009**, *323*, 1566.
(5) Song, K.; Kim, D.; Li, X. S.; Jun, T.; Jeong, Y.; Moon, J. *J. Mater. Chem.* **2009**, *19*, 8881.
(6) Nomura, K.; Takagi, A.; Kamiya, T.; Ohta, H.; Hirano, M.; Hosono, H. *Jpn. J. Appl. Phys.* **2006**, *45*, 4303.
(7) Fortunato, E.; Barquinha, P.; Pimentel, A.; Goncalves, A.; Lavareda, G.; Aguas, H.; Ferreira, I.; Cavalho, C. N.; Pereira, L.; Martins, R. *J. Non-Cryst. Solids* **2004**, *338*, 806.
(8) Kim, H.; Byme, P. D.; Facchetti, A.; Marks, T. J. *J. Am. Chem. Soc.* **2008**, *130*, 12580.
(9) Yaglioglu, B.; Yeom, H. Y.; Beresford, R.; Paine, D. C. *Appl. Phys. Lett.* **2006**, *89*, 062103.
(10) Hoffman, R. L.; Norris, B. J.; Wager, J. F. *Appl. Phys. Lett.* **2003**, *82*, 733.
(11) Jeong, S.; Jeong, Y.; Moon, J. *J. Phys. Chem. C* **2008**, *112*, 30.
(12) Jeong, Y.; Song, K.; Kim, D.; Koo, C. Y.; Moon, J. *J. Electrochem. Soc.* **2009**, *156*, H808.
(13) Hosono, H. *J. Non-Cryst. Solids* **2006**, *352*, 851.
(14) Kotsis, K.; Staemmler, V. *Phys. Chem. Chem. Phys.* **2006**, *8*, 1490.
(15) Cao, H. T.; Pei, Z. L.; Gong, J.; Sun, C.; Huang, R. F.; Wen, L. S. *J. Solid State Chem.* **2004**, *177*, 1480.
(16) Eremenko, A. M.; Smirnova, N. P.; Tropinov, A. G.; Chuiko, A. A. *Theor. Exp. Chem.* **1982**, *18*, 106.
(17) Schneider, J. J.; Hoffmann, R. C.; Engstler, J.; Dilfer, S.; Klyszcz, A.; Erdem, E.; Jakes, P.; Eichel, R. A. *J. Mater. Chem.* **2009**, *19*, 1449.
(18) Meyer, B. K.; Alves, H.; Hofmann, D. M.; Kriegseis, W.; Forster, D.; Bertram, F.; Chreisten, J.; Hoffmann, A.; Strassburg, M.; Dworzak, M.; Haboeck, U.; Rodina, A. V. *Phys. Status Solidi* **2004**, *241*, 231.
(19) Orlinskii, S. B.; Schmidt, J.; Baranov, P. G.; Lorrmann, V.; Riedel, I. *Phys. Rev. B.* **2008**, *77*, 115334.
(20) López, T.; Garcia-Cruz, I.; Gómez, R. *J. Catal.* **1991**, *127*, 75.
(21) Smith, R.; Tench, A. J. *Chem. Commun.* **1968**, 1113.
(22) Tench, A. J.; Holroyd, P. *Chem. Commun.* **1968**, 471.
(23) Wang, J. A.; Novaro, O.; Bokhimi, X.; López, T.; Gómez, R.; Navarrete, J.; Llanos, M. E.; López-Salinas, E. *Mater. Lett.* **1998**, *35*, 317.
(24) Livage, J.; Henry, M. In *Ultrastructure Processing of Advanced Ceramics*; Ulrich, D. R., Ed.; Wiley: New York, 1988, p 183.

AM900787K